ARTICLE

OPEN

Check for updates

Deviations from Taylor's frozen hypothesis and scaling laws in inhomogeneous jet flows

Sukesh Roy[1✉], Joseph D. Miller[2] & Gemunu H. Gunaratne [3✉]

Difficulties in studying turbulent flows stem, in part, from the lack of high-frequency, high-resolution measurements to interrogate small-scale structures and their rapid evolution. We present analysis of data from experiments employing a burst-mode laser system to capture both spatially resolved velocity fields and their dynamics using high-resolution particle image velocimetry measurements at 100 kHz. We show directly that velocity fluctuations in axisymmetric jet flows are inhomogeneous and anisotropic. The peak of the time-delayed cross correlation function decays exponentially in time and its velocity is smaller than the convection velocity; thus, Taylor's frozen hypothesis fails to generalize for these inhomogeneous flows. Structure functions are isotropic only at small distances. They exhibit extended self-similarity, but no inertial range is found where the Kolmogorov $\frac{2}{3}$-law is satisfied. Spectral-energy density of the flow, although anisotropic, is consistent with the Kolmogorov–Obukhov $\frac{5}{3}$-law in the flow direction.

[1] Spectral Energies, LLC, Beavercreek, OH, USA. [2] Air Force Research Laboratory, Wright-Patterson Air Force Base, Dayton, OH, USA. [3] Department of Physics, University of Houston, Houston, TX, USA. ✉email: sukesh.roy@spectralenergies.com; gemunu@uh.edu

Turbulent flows exhibit rapid, irregular spatial and temporal variations in flow velocity fields, whose statistical features are used to characterize turbulence and study its evolution under external changes implemented on the flow. For example, time-averaged velocity fields of turbulent flows can be studied as a function of the Reynold's number $Re = vL_s/v$, where v and L_s are characteristic flow velocity and length scale in the flow, and v the kinematic viscosity[1,2]. The flow transitions from laminar to turbulent as Re increases beyond a threshold. The dynamics of the consequent small-scale structures in turbulent flows are chaotic and are typically characterized through appropriate statistical objects such as cross-correlation coefficients and structure functions[2].

Most theoretical developments on turbulence are predicated on general considerations on energy transmission between scales[3–5]. Specifically, it is assumed that a hierarchy of eddies of different scales acts as intermediaries in energy transmission[6]. Eddies whose size is larger than the Taylor microscale $\lambda = \sqrt{10}L_s Re^{-1/2}$ transmit the entire energy to smaller scales; viscous dissipation is only active at scales smaller than λ[7]. The smallest scale of turbulent flow is the Kolmogorov scale $\eta = L_s Re^{-3/4}$, by which point viscosity has induced complete energy dissipation[3]. The derivation of observed facets of statistical objects requires an additional assumption that for sufficiently large Re, small-scale turbulence is isotropic and homogeneous[3]. This assumption is justified by noting the reduction of inhomogeneity and anisotropy during the energy transfer between scales is dominated by the chaotic nature of the flow[2]. Under these conditions dimensional analysis yields two celebrated results: (1) the "$\frac{2}{3}$-law," on the growth of structure functions and (2) the "$\frac{5}{3}$-law" on the decay in spectral-energy density[2,3,5]. Although these predictions have been experimentally verified in some configurations[8], anomalous scaling of higher order structure functions[9] and anisotropic effects[10–12] have been reported in others.

Scaling laws are expected to hold only at sufficiently high Reynolds numbers. Since Taylor and Kolmogorov scales decrease with increasing Re, experimental validation of the scaling laws require flow velocity measurements at suitably high spatial and temporal resolution. This has been a major challenge for testing scaling laws. Experimental tests have relied on Taylor's frozen hypothesis, that in homogeneous flows turbulent fluctuations propagate downstream with no change[7,13,14]. Under this scenario,

high-frequency single-point measurements, for example using hot-wire anemometry, can be used to infer spatial variations in velocity fields, permitting tests of scaling laws. However, whether the isotropy and homogeneity of velocity fields at small scales is valid in configurations that are inhomogeneous at large scales, and if Taylor's hypothesis and scaling laws are valid in such configurations remains to be tested. Here, the need for high-resolution, high-frequency measurements of flow fields cannot be circumvented.

The critical technology that facilitated the resolution of the turbulent flow in both spatial and temporal domains was the development of a long-duration (100-ms), high-energy burst-mode laser capable of producing pairs of pulses at a rate of 5 kHz to 1 MHz[15,16]. It permitted the performance of two-dimensional velocity measurements employing particle image velocimetry (PIV) at a rate of 100 kHz and a resolution of flow features (both spatially and temporally) almost down to the Taylor micro-scale for $Re < 80,000$. For example, at 100 kHz in the present study, we acquired ~ 8500 velocity-field snapshots within the 100-ms duration. Turbulent jet flows of Re between 21,000 and 78,000 emanated from a cylindrical inlet of diameter $D = 4.7$ mm. As it moved downstream, the axisymmetric flow expanded (nearly) linearly. Velocity measurements at 100 kHz were made on a grid of 51×67 of lattice size 0.268 mm placed symmetrically in an axial plane approximately $13D$ downstream of the inlet, as shown in Fig. 1a. Figure 1b is a snapshot of the flow velocity field for $Re \approx 78,000$. The Taylor micro-scale and the Kolmogorov scale for the flow are 165 μm and 3 μm, respectively. Statistical objects were computed through time averages, which were assumed to be reliable surrogates for ensemble averages[2]. Since the lattice size ~ Taylor micro-scale, nearly the entire inertial scale could be examined. The PIV measurements were recorded once it was determined that the flow had stabilized and the seed density was sufficiently high throughout the flow (see Methods). That statistical objects had converged was verified by computing them over different time intervals.

We show directly that turbulent fluctuations in the jet flow are neither isotropic nor homogeneous. We also show that the peak of the time-delayed cross-correlation coefficient decays exponentially in time and flows slower than the convection velocity. Thus, we infer that Taylor's frozen hypothesis[7] is modified in the inhomogeneous jet flow. Further, structure functions fail to
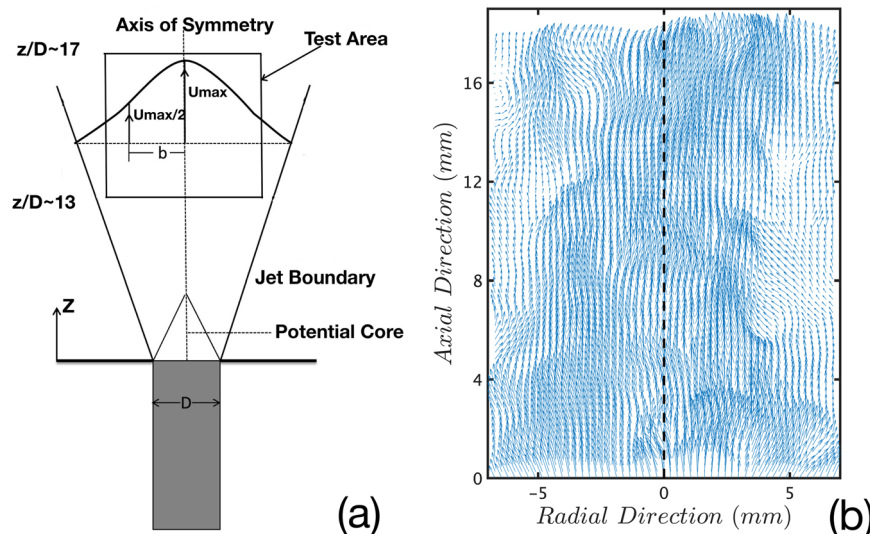

Fig. 1 Experimental setup and flow fields. a Axisymmetric jet flow about the symmetry axis z is generated by N_2 gas ejected from cylinder of radius $D = 4.7$ mm. Flow velocity in a plane normal to the symmetry axis peaks on the axis and is denoted U_{max}. Rectangular axial region of size 13.4 × 17.7 mm where velocity measurements were made was approximately $13D$ downstream (i.e.,z-direction) of inlet. **b** Snapshot of velocity field for flow of $Re \approx 78,000$.

exhibit an inertial range where they scale[3]. However, extended self-similarity[17] is found to hold except at small distances; thus, once the form of the second-order structure function is established, that of higher-order structure functions can be approximated. Finally, spectral energy densities are anisotropic but are shown to be consistent with the Kolmogorov–Obhukov law[4,5] in the flow direction.

Results and discussion

Inhomogeneity of velocity fluctuations. Denote the time average of the velocity field $\mathbf{v}(\mathbf{R}; t)$ and its deviation from the mean by $\bar{v}(\mathbf{R})$ and $\mathbf{v}'(\mathbf{R}; t)$ respectively, where $\mathbf{R}$ is measured from the center of the near-boundary. The axial and radial projections $\bar{v}_z(\mathbf{R})$ and $\bar{v}_r(\mathbf{R})$ are given by the Tollmien solution[18,19] derived by expressing the Reynold's equation[1] in cylindrical polar coordinates (r, θ, z) and noting that for sufficiently large Re, the viscous stresses are insignificant compared to turbulent shear stresses. As shown in Supplementary Note 2, the experimental velocity fields satisfy the Tollmien solution, which is neither isotropic nor homogeneous. It has generally been posited that even in such cases, small-scale turbulent flows are isotropic and homogeneous at sufficiently large Re[2]. However, more recent work has cautioned against the conjecture for inhomogeneous flows[20].

We implement a pre-processing step to eliminate recurrent features of the flow, whose origins may lie in imperfections of the experimental set-up, acoustic reflections from laboratory walls, etc. Theoretical approaches consider only the remaining non-recurrent facets of a flow. The implementation, based on robust mode analysis[21], is outlined in Supplementary Note 1. For jet flow at $Re \approx 78,000$, we find, and eliminate, one recurrent global mode of period 0.72 ms.

One significant advantage of spatio-temporal jet-flow data is that they can be used to perform a direct tests of the symmetries of $\mathbf{v}'(\mathbf{R}; t)$ down to the scale of the lattice (~ 0.27 mm)[16,22]. These velocity fluctuations are found to be both anisotropic and inhomogeneous. Specifically, the standard deviations of $v'_z(r, z; t)$ and $v'_r(r, z; t)$ decrease along the flow axis and are nearly constant in the radial direction except near the edge of the domain, where they decay. As shown in Supplementary Note 3, the corresponding turbulent intensity $\mathcal{T} \equiv \sigma[v'_z]/\bar{v}_z$[14] is nearly constant along the z axis and increases from ~0.1 to ~0.6 in the radial direction.

Cross-correlation coefficient. Incompressibility of the fluid, diffusion, as well as the presence of tube-like vortex structures[23,24] induce correlations between velocity fluctuations at neighboring sites in turbulent flows. Among measures used for quantitative assessment are the time-delayed cross-correlation coefficient

$$C(\mathbf{R}, \mathbf{R}'; \tau) = \frac{\langle \mathbf{v}'(\mathbf{R}; t) \cdot \mathbf{v}'(\mathbf{R}'; t + \tau) \rangle_t}{\sigma[\mathbf{v}'(\mathbf{R})]\sigma[\mathbf{v}'(\mathbf{R}')]}, \quad (1)$$

and the analogous quantities $C_z(\mathbf{R}, \mathbf{R}'; \tau)$ and $C_r(\mathbf{R}, \mathbf{R}'; \tau)$ for the axial and radial velocity components. Here $\sigma[\mathbf{v}'(\mathbf{R})]$ is the standard deviation of the signal $\mathbf{v}'(\mathbf{R}; t)$. Note that $C(\mathbf{R}, \mathbf{R}'; \tau = 0) \to 1$ as $|\mathbf{R}' - \mathbf{R}| \to 0$. When Taylor's frozen hypothesis[7,13,14] is valid, $C(\mathbf{R}, \mathbf{R}'; \tau) = 1$ for sufficiently nearby points $\mathbf{R}'$ downstream of $\mathbf{R}$ for $\tau = |\mathbf{R}' - \mathbf{R}|/\bar{v}_z$. Its validity for inhomogeneous flows has been debated[20,25]. In the absence of a theoretical framework, spatio-temporal data is indispensable to establish, if and how the hypothesis is modified for inhomogeneous flows. Analyses outlined below were conducted on recordings from four 15 ms intervals (i.e., 1500 snapshots) of the data; the error bars are standard deviations.

Figure 2 summarizes features of the cross-correlation coefficient with $\mathbf{R} = \mathbf{0} \equiv (0, 0)$ for jet flows at $Re \approx 78,000$. Figure 2(a) shows

three snapshots of $C(\mathbf{0}, \mathbf{R}'; \tau)$, which is seen to contain a growing downstream-flowing peak. Denote the mean flow velocity at the n'th lattice site on the symmetry axis as $\bar{v}_z(n)$, which, as shown in Supplementary Note 3, is a decreasing function of n. The time t_n for a signal at the origin to reach the n'th lattice site is bounded by $\sum_{m=1}^{n} \delta/\bar{v}_z(m) < t_n < \sum_{m=0}^{n-1} \delta/\bar{v}_z(m)$, where $\delta = 0.268$ mm is the lattice size. The bounds are indistinguishable, and the line $(t_n, n\delta)$ is shown in red in Fig. 2(b). The position of the peak, shown by blue diamonds in Fig. 2(b), flows at ~80% of this convection velocity[26], consistent with prior studies[27–30]. (Deviations are found at off-axial sites as well, but with differing ratio of velocities.) The difference is most easily explained through Lagrangian flow; i.e., description from a frame co-moving with the axial flow. As any velocity fluctuation diffuses to neighboring sites, where the flow-velocity is negative (since the velocity is highest on the symmetry axis), thus dragging the disturbance backward. The deviation of the peak velocity from the convection velocity is thus due to the inhomogeneity in mean flow, as given by the Tollmien solution[18].

A second modification to Taylor's hypothesis, under which the peak intensity remains 1, is an exponential decay of the peak, see Fig. 2d. We propose that it originates from the reversal of velocity fluctuations required to maintain an average flow velocity at a site. The conjecture is motivated by a similar exponential decay (following transients) in the paradigmatic mean-reversing stochastic dynamics, the Ornstein–Uhlenbeck process[31]. Since mean reversal of velocity fluctuations is necessary to maintain the mean flow velocity at a location, it is a reasonable conjecture that the exponential decay of correlations will also hold for homogeneous flows, although experimental validation at small distances may be difficult. Figure 2c shows that the growth of the peak-width is linear both in the flow direction and normal to it. Although differences in the velocity of the correlation peak and the convection velocity have been reported in prior studies[13,25,32,33], to the best of the authors' knowledge, this is the first quantitative assessment of the decay of the peak in inhomogeneous flows.

Figure 2e shows an interesting observation. Due to the anisotropic growth rate and shape of the intense regions of $C(\mathbf{0}, \mathbf{R}'; \tau)$, the peak along any direction within a cone is seen to be approximately independent of the direction. The four lines are the peak locations as a function of time in directions bearing angles $\theta = 0$ (flow direction), $\theta = \tan^{-1}(1/6) = 9.46^o$, $\theta = \tan^{-1}(1/5) = 11.31^o$, and $\theta = \tan^{-1}(1/4) = 14.04^o$ to the flow direction, the lines being shifted for clarity. The slopes in all directions are nearly identical. (This direction-independence fails for smaller Reynolds numbers, see Supplementary Fig. 9e.) However, as seen from Fig. 2d, the decay in the peak-intensity is not isotropic; it decreases faster as the deviation from the flow direction increases.

Spectral energy density. Velocity fluctuations in turbulent flows can be quantified via spectral components of the "energy field" $E(\mathbf{R}) = \frac{1}{2} \langle \mathbf{v}(\mathbf{R}, t) \cdot \mathbf{v}(\mathbf{R}, t) \rangle_t$ of a unit mass of fluid[4,5]. When $E(\mathbf{R})$ is isotropic, dimensional considerations have been used to show that the spectral energy density scales as $\hat{E}(k) \sim k^{-5/3}$ in the inertial range[4,5]. Due to lack of high resolution spatial data, most previous investigations used single-point velocity fluctuations and invoked Taylor's frozen hypothesis to establish the behavior of the Fourier spectrum $\hat{E}(\omega)$ of the time series[16,34]. We wish to test for scaling of spectral energy in axisymmetric jet flow. Dimensional arguments analogous to those in refs. [4,5] show that the axial and radial components $\hat{E}_z$ and $\hat{E}_r$ of the spectral energy will scale as $k_z^{-5/3}$ and $k_r^{-5/3}$, respectively.
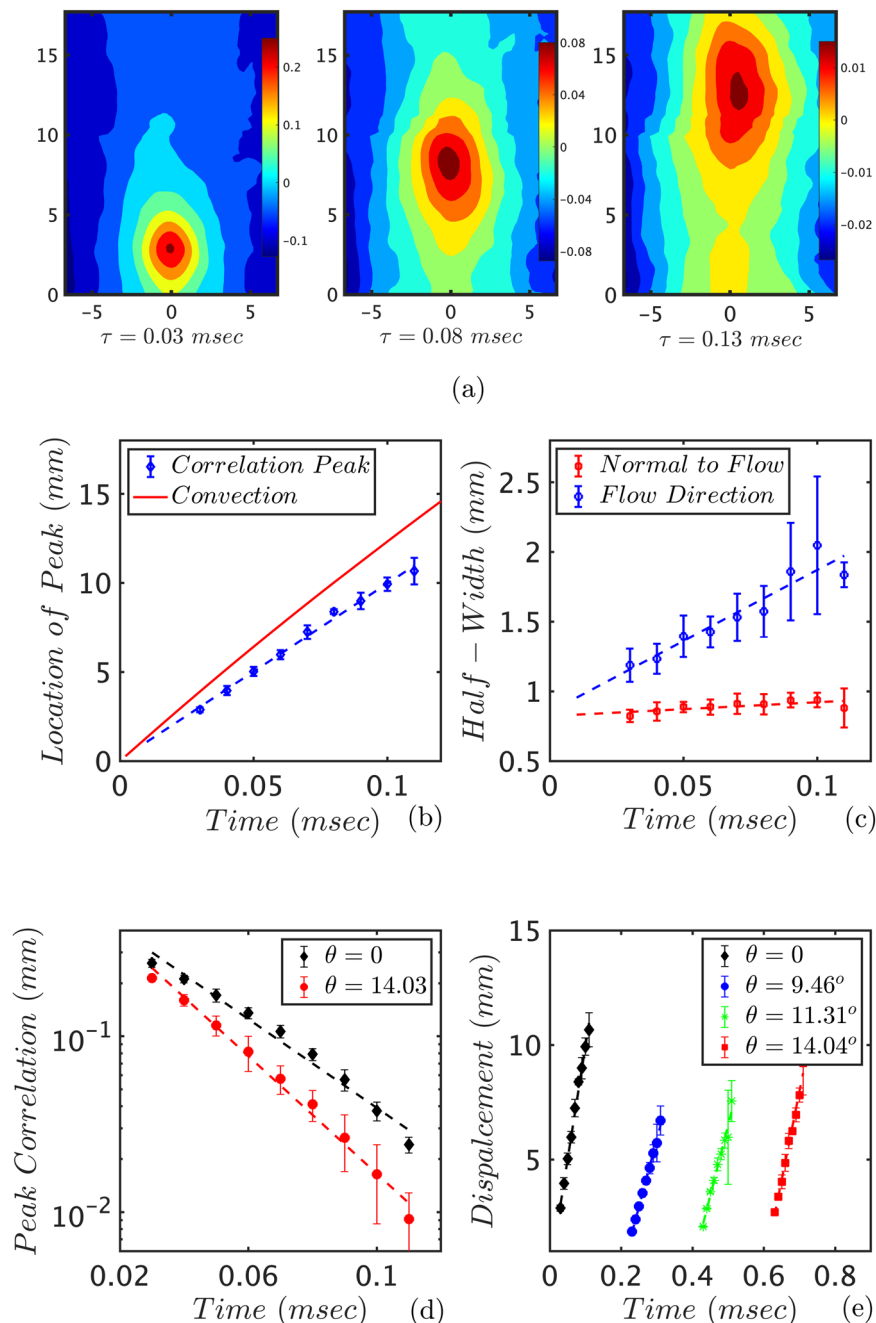
3

Fig. 2 Properties of time-delayed cross-correlation functions. a Three snapshots of the field $C(\mathbf{R} = \mathbf{0}, \mathbf{R}'; \tau)$, whose peak flows downstream and broadens in time. Distances are given in mm and the center of the near-boundary is chosen as the origin. Panels **b**–**e** show mean values (symbols) and standard deviations (error bars) of variables computed from four non-overlapping subintervals, each of 1500 snapshots. **b** The downstream velocity of the peak (blue diamonds) is smaller than the convection velocity (red line). **c** The width of the peak, both in the flow direction (blue circles) and normal to it (red circles), grows linearly in time. **d** The peak $P_z(\tau)$ (flow direction: $\theta = 0$, black diamonds) decays exponentially in time. **e** Velocity of the peak is nearly independent of the direction within a cone. The lines (shifted for clarity) show the peak locations as a function of time for the flow direction (black diamonds) and for directions $\theta = \tan^{-1}(1/6)$ (blue circles), $\tan^{-1}(1/5)$ (green crosses), and $\tan^{-1}(1/4)$ (red squares) from the flow axis. However, as seen in **d**, the peak intensity decays faster away from the flow direction (red circles).

The spatio-temporal velocity fields permit a direct computation of $E(\mathbf{R})$, which as seen from Fig. 3a, is not isotropic. Prior to computing the spectrum, we extend $E(\mathbf{R})$ in both the z and the r directions so that the extended field is periodic. The Fourier transform is performed on this extended field with periodic boundary conditions in order to minimize spurious spectral components. The z extension is a reflection across $z_{\max}$. In the r direction, a linear transformation is applied on each z row of $E(\mathbf{R})$ so that the transformed field vanishes at the ends; it is then extended by reflection and multiplication by -1.

Since $E(\mathbf{R})$ for the jet flow is anisotropic, it is necessary to analyze the behavior of the 2-dimensional spectral energy density $\hat{E}(k_r, k_z)$. We find that $\hat{E}(k_r, k_z = 0)$ is several orders of magnitude smaller than $\hat{E}(k_r = 0, k_z)$. Figure 3b shows that the latter is consistent with the Kolmogorov–Obukhov[4,5] law.
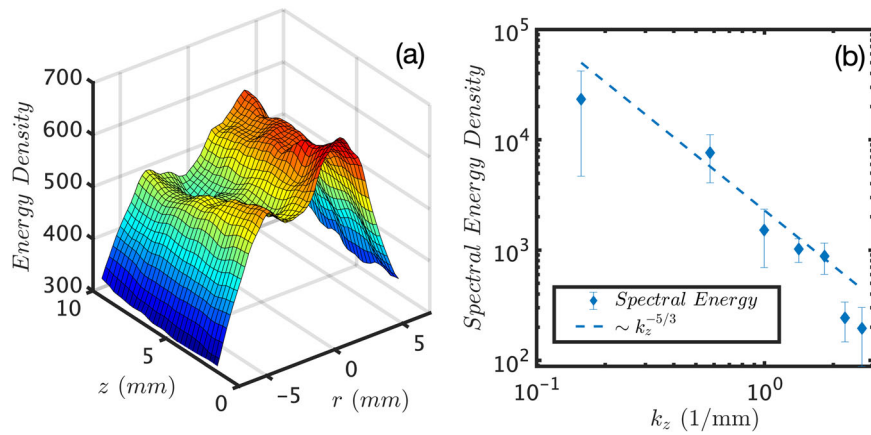
Fig. 3 Energy density and spectral energy density of flow. a Energy density $E(r, z)$ for a jet-flow of $Re \approx 78,000$. **b** Decay of $\hat{E}(k_r = 0, k_z)$ as a function of k_z. Each blue diamond represents the mean of $\hat{E}(k_r = 0, k_z)$ at four successive points and error bars, the associated standard deviations. Dashed line shows Kolmogorov–Obukhov scaling.

Structure functions. High-frequency, high-resolution velocity measurements aid in establishing several interesting statistical characterizations of point-wise and joint velocity-fluctuations in turbulent flows. The results from our analyses, presented in Supplementary Note 3, can be summarized as follows: (a) Point-wise velocity fluctuations, both in the axial (v'_z) and normal (v'_r) directions, are nearly Gaussian distributed. Standard deviations in the axial and normal velocity fluctuations differ; specifically $\sigma(v'_z) = 25.59 \pm 1.51 \, m/s$ and $\sigma(v'_r) = 17.80 \pm 0.51 \, m/s$. Furthermore, $\sigma(v'_z)$ exhibits a slow decay of ~5% over 17.7 mm in the down-flow direction. These observations imply the inhomogeneity and anisotropy of $\mathbf{v}'$. (b) As seen in Supplementary Fig. 4d, cross-correlation between point-wise axial and normal velocity fluctuations increases to the right and decreases to the left of the symmetry axis. This observation indicates that velocity fluctuations are not randomly oriented; the on-axis correlation is ≲0.1. (Although the on-axis correlation should vanish by reflection symmetry, it is only approximately so for the <0.1 s duration of the experimental signal.) (c) As shown in Supplementary Note 4, distributions of pairwise velocity differences $\delta \mathbf{v}' \equiv \mathbf{v}'(\mathbf{R}; t) - \mathbf{v}'(\mathbf{R}'; t)$ are multivariate Gaussian when the two points are far apart, but develop broader tails as points are brought close to each other. In particular, they are nearly bi-exponential at the smallest distances[28,30]. This anomaly may originate from incompressibility and the presence of tube-like vortex structures[23,24]. Figure 2a provides an alternative interpretation: as the peak of the cross-correlation broadens, the strong correlation between velocity fluctuations at two neighboring sites with those at the origin at an earlier time implies the correlation of velocity fluctuations at the two points themselves.

Correlations between velocity fluctuations at neighboring sites can be characterized using the family of structure functions

$$S_\zeta(\mathbf{R}, \mathbf{R}') = \frac{\langle |(\mathbf{v}'(\mathbf{R}; t) - \mathbf{v}'(\mathbf{R}'; t)) \cdot \mathbf{e}_\parallel|^\zeta \rangle_t}{\langle |\mathbf{v}'(\mathbf{R}; t) \cdot \mathbf{e}_\parallel|^\zeta \rangle_t + \langle |\mathbf{v}'(\mathbf{R}'; t) \cdot \mathbf{e}_\parallel|^\zeta \rangle_t}, \quad (2)$$

where $\mathbf{e}_\parallel \equiv \mathbf{e}_\parallel(\mathbf{R}' - \mathbf{R})$ is the unit vector in the direction $(\mathbf{R}' - \mathbf{R})$. Increasing ζ emphasizes larger deviations. We find that structure functions are homogeneous on the symmetry axis, i.e., do not depend on the "origin" $\mathbf{R}$. Our computations of structure functions are implemented on a 60 ms (6000-frame) segment of the flow. The error bars in Fig. 4 represent standard deviations for four different origins $\mathbf{R}$ on the symmetry axis.

Contour plot of $S_1(\mathbf{R}, \mathbf{R}')$, Fig. 4a, shows that it is nearly isotropic when $|\mathbf{R} - \mathbf{R}'|$ is small, but that its growth slows in the flow direction with increasing $|\mathbf{R} - \mathbf{R}'|$. Additional features of $S_\zeta(\mathbf{R}, \mathbf{R}')$ can be inferred from observations on the distributions of velocity fluctuations outlined earlier. They include (a) continuity of velocity fluctuations imply that $S_\zeta(\mathbf{R}, \mathbf{R}') \to 0$ as $|\mathbf{R} - \mathbf{R}'| \to 0$. (b) Since the distribution of velocity fluctuations at $\mathbf{R}$ and $\mathbf{R}'$ are multivariate normal and the $\mathbf{v}'$'s are independent when $|\mathbf{R} - \mathbf{R}'| \to \infty$, the distribution of $\mathbf{v}'(\mathbf{R}; t) - \mathbf{v}'(\mathbf{R}'; t)$ is multivariate normal with a variance–covariance matrix that is the sum of those for the two distributions. Since the variances of the distribution of axial velocity fluctuations are (nearly) constant within the entire domain, it is seen that $S_2(\mathbf{R}, \mathbf{R}') \to 1$ as $|\mathbf{R} - \mathbf{R}'| \to \infty$. (c) In addition, $S_\zeta(\mathbf{R}, \mathbf{R}') \to const.$ as $|\mathbf{R} - \mathbf{R}'| \to \infty$, the limiting value depending on ζ. Specifically, since $\mathbb{E}[|X|^\zeta] = \frac{2^{\zeta/2}}{\sqrt{\pi}} \Gamma\left(\frac{\zeta+1}{2}\right) \sigma^\zeta$ for a centered normal distribution of standard deviation σ, it can be shown that $S_\zeta(\mathbf{R}, \mathbf{R}') \to 2^{\zeta/2-1}$ as $|\mathbf{R} - \mathbf{R}'| \to \infty$.

Figure 4b, c shows the behavior of structure functions in the flow direction. Black diamonds in Fig. 4b are the values of $S_1(z)$, with $z = |\mathbf{R} - \mathbf{R}'|$. Consistent with the limits for $z \to 0$ and $z \to \infty$, we use a 3-parameter fit $S_1(z) = c_1 z^{c_3}/(1 + c_2 z^{c_3})$; the best fit is shown by the black line in Fig. 4b. The blue, red, green, and brown symbols in Fig. 4b represent $S_{1/2}(z)$, $S_2(z)$, $S_3(z)$, and $S_4(z)$, respectively. Next, given $S_\zeta(z) \to 2^{\zeta/2-1}$ when $z \to \infty$, we inquire if $S_\zeta(z)$ will be a power of $S_1(z)$. The conjecture is tested using the "normalized" structure function

$$\mathbb{N}S_\zeta(z) \equiv \frac{S_\zeta(z)}{S_1(z)^\zeta}. \quad (3)$$

The symbols in Fig. 4c, $\mathbb{N}S_{1/2}(z)$, $\mathbb{N}S_2(z)$, $\mathbb{N}S_3(z)$, and $\mathbb{N}S_4(z)$, illustrate that a power-relationship does hold for large z, the limiting value being consistent with $\mathbb{N}S_\zeta(z) = 2^{\zeta-1}$ (thin solid lines), except at the largest ζ. This is an example of extended self-similarity[17,35]; it motivates us to inquire how well $S_\zeta(z)$ is approximated by $2^{\zeta-1}S_1(z)^\zeta$ in the entire range. The blue, red, green, and brown lines in Fig. 4b show that the approximation does hold over the entire domain, but weakens as ζ increases. It is shown in Supplementary Note 5 that (a) the discrepancy at large z can be attributed to small correlations and differences in point-wise standard deviations, and (b) the behavior for small z can be found using the near bi-exponential form of the distribution of velocity differentials.

The well-known Kolmogorov "$\frac{2}{3}$-law" states that for highly turbulent homogeneous and isotropic flows, there is an inertial
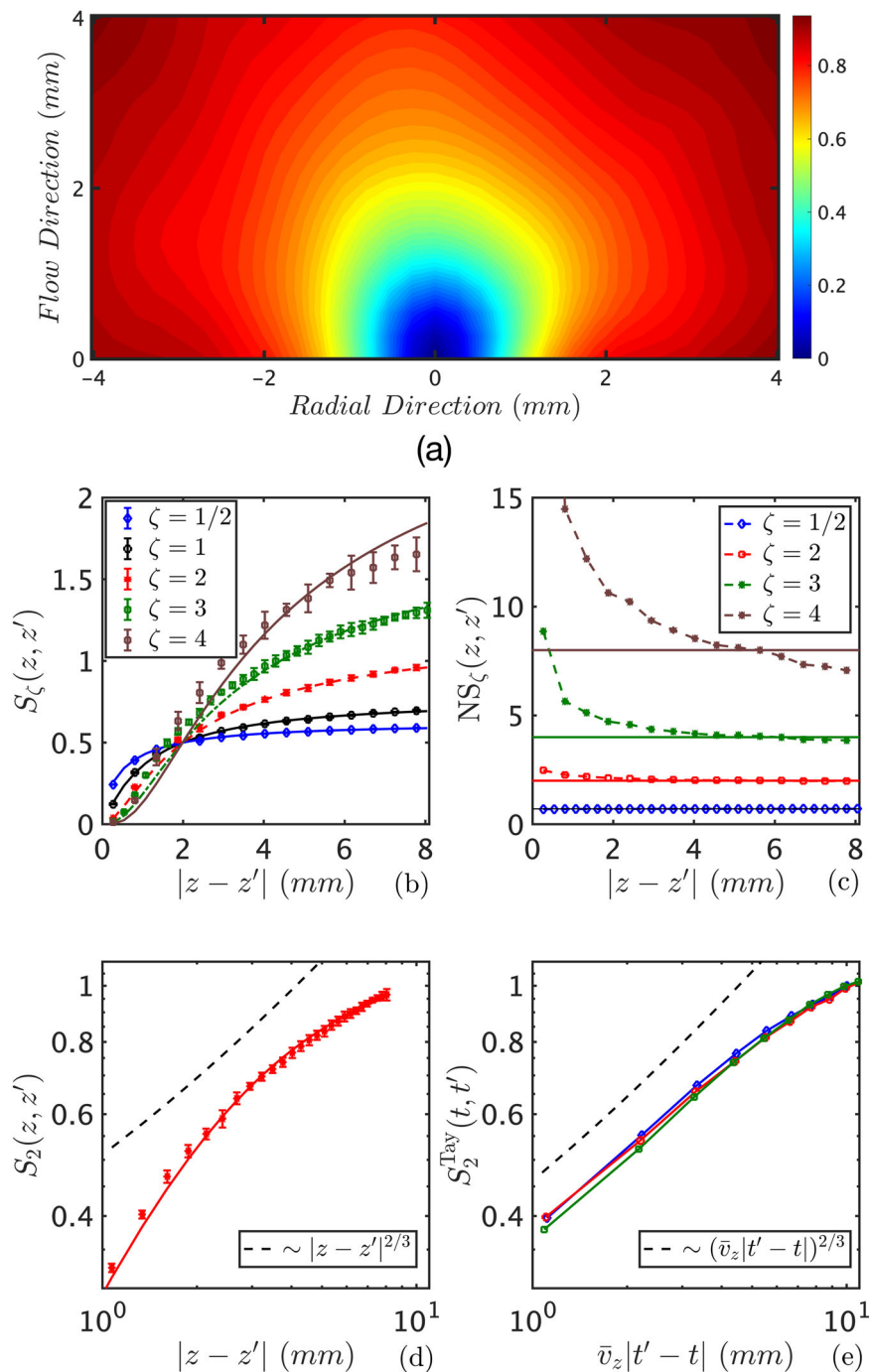
Fig. 4 Properties of structure functions. a Contour plot for $S_1(\mathbf{R}, \mathbf{R}')$ shows that it is nearly isotropic when $d = |\mathbf{R}' - \mathbf{R}|$ is small, but that the growth slows in the flow direction as d increases. Panels **b**–**e** show mean values (symbols) and standard deviations (error bars) for variables computed using 6000-frame segments with four distinct origins $\mathbf{R}$ on the symmetry axis. **b** The symbols show $S_{1/2}(\mathbf{R}, \mathbf{R}')$ (blue diamonds), $S_1(\mathbf{R}, \mathbf{R}')$ (black circles), $S_2(\mathbf{R}, \mathbf{R}')$ (red crosses), $S_3(\mathbf{R}, \mathbf{R}')$ (green squares), and $S_4(\mathbf{R}, \mathbf{R}')$ (brown stars) in the flow direction. The black line is the best fit of the data $S_1(z)$ for a functional form $S_1(z) = c_1 z^{c_3}/(1 + c_2 z^{c_3})$ that satisfies the conditions for $|\mathbf{R} - \mathbf{R}'| \to 0$ and $|\mathbf{R} - \mathbf{R}'| \to \infty$. **c** Normalized structure functions $\mathbb{N}S_\zeta(z)$ for $\zeta = 1/2, 2, 3,$ and 4, showing the validity of extended self-similarity[17,35] for large $|z - z'|$. Extended self-similarity suggests that $S_\zeta(z) \approx 2^{\zeta-1} S_1(z)^\zeta$. These are the lines shown in **b**. **d** $S_2(z, z')$ does not show an inertial range where the Kolmogorov $\frac{2}{3}$-law holds. **e** An assessment of the structure function from a single-point time series invoking Taylor's hypothesis is better approximated by the $\frac{2}{3}$-law.

range, terminating at the Taylor micro-scale, where $S_2(\mathbf{R}, \mathbf{R}')$ is isotropic and scales like $|\mathbf{R}' - \mathbf{R}|^{2/3}$[2,3], and that higher-order structure functions scale as $S_\zeta(\mathbf{R}, \mathbf{R}') \sim |\mathbf{R}' - \mathbf{R}|^{\zeta/3}$. Experimental evidence for these claims, many of which are based on Taylor's frozen hypothesis, have not been conclusive. For example, while several studies appear to affirm isotropy of structure functions[36,37], others report anisotropy[38,39]. An inertial range is not observed in some studies on turbulent flows[30] and simulations[17], while it is found in others[9,40,41].

With high-resolution spatio-temporal flow fields, we are in a position to perform direct and indirect (i.e., based on Taylor's frozen hypothesis) tests of Kolmogorov scaling in the anisotropic and inhomogeneous jet flow. Due to experimental noise and

limitations on resolution, estimations of higher order moments are not reliable. The symbols in Fig. 4d show $S_2(z, z')$ and the line through them the best fit to a functional form $S_2(z) = c_1 z^{c_3}/(1 + c_2 z^{c_3})$; the dashed line is the $\frac{2}{3}$-law. No inertial range is found for our data. Transverse structure functions exhibit similar features, as summarized in Supplementary Note 6 and Supplementary Figs. 7 and 8.

It has been conjectured that inhomogeneity and anisotropy induces deviations from a single scaling index[9], and that structure functions scale only within irreducible sectors of the $SO(3)$ symmetry group[10,42–44]. The axisymmetric jet flows reported here show no scaling even within irreducible sectors.

Next, we inquire if use of Taylor's frozen hypothesis can contribute to experimental observations of an inertial range[9,40,41]. Under the scenario, single point velocity measurements at a location $\mathbf{R} = (0, z)$ on the symmetry axis can be used to evaluate the structure function in the flow-direction via

$$S_2^{\text{Tay}}(t, t') = \frac{\langle |v_z'(z; t) - v_z'(z; t'))|^2 \rangle_t}{2\langle |v_z'(z; t)|^2 \rangle_t}. \tag{4}$$

In Fig. 4e, we show the form of the structure function at three locations as a function of the effective distance $\bar{v}_z|t' - t|$, where $\bar{v}_z$ is the mean flow velocity at $\mathbf{R}$. Since the time interval between observations is 0.01 ms and the fluid speed in the flow direction is ~130 m/s, the smallest effective distance accessible from the data is ≈1.3 mm; given that the Taylor micro-scale is ≈165 μm, we are unable to access the lower distances in the inertial scale. An inertial range cannot be observed, but $S_2^{\text{Tay}}(t, t')$ shows a closer agreement to the $\frac{2}{3}$-law than $S_2(\mathbf{R}, \mathbf{R}')$.

Conclusions
A signature of turbulent flows is rapid chaotic variations in flow velocities, and the flows are characterized through statistical objects of their fluctuations. Theoretical analysis of these objects are based primarily on energy transmission between scales, leading to the Kolmogorov $\frac{2}{3}$-law and the Kolmogorov–Obhukov $\frac{5}{3}$-law. Reynolds numbers where these laws are predicted to hold are extremely high, and the flows contain structures down to very small scales. A major challenge for experimental tests of the scaling laws is measurements of flow fields at sufficiently high frequency and spatial resolution. Studies of homogeneous turbulence has been predicated on the use of Taylor's frozen hypothesis which permits the inference of the relevant spatial variations via the use of high-frequency single or multi-point measurements. Whether these inferences generalize to the more common inhomogeneous flows was the issue that motivated the present study.

The acquisition of high-resolution spatio-temporal velocity fields was made through a long-duration (100-ms), high-energy burst-mode laser, permitting their extraction at a frequency of 100 kHz[15]. This rate of measurements permitted the study of axisymmetric jet flows up to Reynolds numbers ~80,000. We showed explicitly that both the mean flow and velocity fluctuations in these flows are inhomogeneous and anisotropic. One of our inquiries was if and how Taylor's hypothesis is altered. We found that the peak in the auto-correlation function flows at a rate that differs from the convection velocity and attributed it to non-uniformity of the mean flow. The peak correlation was found to decay exponentially in time. We argued that the observation can be attributed to mean-reversal of velocity fluctuations, which suggests that such a decay will persist in homogeneous flows as well, even at short distances. Next we used the flow fields to test if scaling of structure functions[4,5] and spectral energy density will continue in inhomogeneous flows. Even though extended self-similarity[17,35] holds except at small distances, we failed to find an inertial range where the Kolmogorov $\frac{2}{3}$-law[3] holds. The decay of

the axial component of the spectral energy density is consistent with the Kolmogorov–Obukhov law[4,5].

Methods
The N_2-jet, inserted through a cylindrical inlet of diameter 4.7 mm with a flow rate set by a mass flow controller (Alicat, MCR), expands axi-symmetrically into ambient stagnant air. The 2D velocity measurements are made on a grid inside the boundary of the expanding jet. Reynold's numbers at the inlet for our experiments range from 21,000–78,000 (see Supplementary Note 7).

Velocity measurements are made using high-speed time-resolved PIV, whose acquisition rates in our system are limited primarily by repetition rates of laser sources and infrared camera memory. Wth an extended-duration dual-pulse burst-mode laser[16] we are able to acquire the flow field measurements at 100 kHz over a duration of 0.1 s. The flow field was visualized using DEHS particles of diameter 0.25 μm. Under these conditions the motion of the particles is passive[16], and thus their flow will represent that of the fluid faithfully. The PIV resolution was made for each condition using the standard interpretation[22], requiring the vector correlation size (537 μm), laser sheet thickness (500 μm), and time resolution between correlated images (2 μs). For conditions analyzed, the spatial resolution varies from 266 μm to 277 μm. Ref. [16] provides a detailed analysis of particle motion and rigorous definitions of spatial and temporal resolution. For all cases, a standard definition of resolution was used, i.e., the Taylor micro-scale wave-vector at which the correction ratio of the squared spectral filtering function fell to 0.7. This can be interpreted as the point at which corrections of less than 30% are required to the spectral density tensor, in agreement with the standard work of Lavoie[22]. However, if a more stringent definition is applied (e.g., corrections less than 10%), then the effective spatial resolution would decrease.

The integral length scale was estimated as the product of the mean convective velocity and the measured integral time scale[45]. The time-scale was measured using the exponential decay of the temporal autocorrelation function[45]; the length-scale Λ was expressed in terms of the turbulence intensity (estimated from the standard deviation σ_1 in the axial direction) and the dissipation rate ε was estimated using $\Lambda \approx \sigma_1^3/\varepsilon$[46]. The Taylor micro-scale was estimated by substituting this expression, yielding $\lambda \approx \sqrt{15\nu\Lambda/\sigma_1}$, and is a function of derived and measurable axial quantities in the experiment: kinematic viscosity ν, Λ, and σ_1. The Kolmogorov scale was estimated using the approximation $\eta \approx (\nu^3\Lambda/\sigma_1^3)^{1/4}$[46]. Further details of these calculations can be found in ref. [45].

The velocity measurements are made on a 67×51 grid placed symmetrically on an axial cross-section, as illustrated schematically in Fig. 1a. There were a very few instances (~0.01%) where both the recorded axial and radial speeds vanish, indicating that the site was not seeded. (We find no cases where only one component vanishes.) Each such recording is replaced by the mean of the corresponding velocities at the same location in the time steps immediately preceding and following the instance.

Data availability
The spatio-temporal flow velocity data that support the findings of this study, in Matlab format, have been deposited in "figshare.com", with the accession code "10.6084/m9.figshare. 12789926." Grid points x and y of the 51×67 lattice and the velocity fields $u(x, y, t)$ and $v(x, y, t)$ in the x and y directions are given for jet flows at Reynolds numbers 21,000, 26,200, 31,500, 47,200 62,300, and 77,900.

Code availability
Computer codes used to analyze the data will be provided upon request.

References
1. Reynolds, O. On the dynamical theory of incompressible viscous fluids and the determination of the criterion. *Philos. Trans. R. Soc. Lond.* **186**, 123–161 (1894).
2. Monin, A. S. & Yaglom, A. M. *Statistical Fluid Mechanics, Mechanics of Turbulence* Vol. I (Dover Publications, Inc., 1971).
3. Kolmogorov, A. N. Local structure of turbulence in an incompressible fluid at very high Reynolds numbers. *Dokl. Akad. Naud. SSSR* **30**, 299–303 (1941).
4. Kolmogorov, A. N. Energy dissipation in locally isotropic turbulence. *Dokl. Akad. Naud. SSSR* **32**, 19–21 (1941).
5. Obukhov, A. M. Energy distribution in the spectrum of a turbulent flow. *Izvestiya Akad. Nauk. SSSR, Ser. Geogr. Geofiz.* **4-5**, 453–466 (1941).
6. Richardson, L. F. *Weather Prediction by Numerical Processes* (Cambridge University Press, 1922).
7. Taylor, G. I. The spectrum of turbulence. *Proc. R. Soc. London, Ser. A* **164**, 476 (1938).
8. Saddoughi, S. G. & Veeravalli, S. V. Local isotropy in turbulent boundary layers at high Reynold's number. *J. Fluid Mech.* **268**, 333–372 (1994).

9. Anselmet, F., Gagne, Y., Hopfinger, E. J. & Antonia, R. High-order velocity structure functions in turbulent shear flows. *J. Fluid Mech.* **140**, 63–89 (1984).

10. Biferale, L. & Procaccia, I. Anisotropy in turbulent flows and in turbulent transport. *Phys. Rep.* **414**, 43–164 (2005).

11. Procaccia, I. & Sreenivasan, K. R. The state of the art in hydrodynamic turbulence: past successes and future challenges. *Phys. D-Nonlinear Phenom.* **237**, 2167–2183 (2008).

12. Sreenivasan, K. R. & Druva, B. Is there scaling in high-Reynolds-number turbulence? *Prog. Theor. Phys. Suppl.* **130**, 103–120 (1998).

13. Lŕvov, V. S., Pomyalov, A. & Procaccia, I. Temporal surrogates of spatio-temporal turbulent statistics: the Taylor hypothesis revisited. *Phys. Rev. E* **60**, 4175–4184 (1999).

14. Belmonte, A., Martin, B. & Goldburg, W. I. Experimental study of Taylor's hypothesis in a turbulent soap film. *Phys. Fluids* **12**, 835–845 (2000).

15. Slipchenko, M. et al. 100-kHz, 100-ms, 400-J burst-mode laser with dual-wavelength diode-pumped amplifiers. *Opt. Lett.* **39**, 4735–4738 (2014).

16. Miller, J. D. et al. Spatiotemporal analysis of turbulent jets enabled by 100-kHz, 100-ms burst-mode particle image velocimetry. *Exp. Fluids* **57**, 192 (2016).

17. Benzi, R. et al. Extended self-similarity in turbulent flows. *Phys. Rev. E* **48**, R29–R32 (1993).

18. Tollmien, W. Berechnung turbulenter ausbreitungsvorgänge. *Zs. Angew. Math. Mech.* **6**, 468–478 (1926).

19. Rajaratnam, N. *Turbulent Jets* (Elsevier Scientific Publishing Company, 1976).

20. Frisch, U. *Turbulence: the Legacy of A. N. Kolmogorov* (Cambridge University Press, 1995).

21. Hua, J.-C., Gunaratne, G. H., Talley, D. G., Gord, J. R. & Roy, S. Dynamic-mode decomposition based analysis of shear coaxial jets with and without transverse acoustic driving. *J. Fluid Mech.* **790**, 5–32 (2016).

22. Lavoie, P., Avallone, G., De Gregorio, F., Romano, G. P. & Antonia, R. A. Spatial resolution of PIV for the measurement of turbulence. *Exp. Fluids* **43**, 39–51 (2007).

23. Siggia, E. Numerical study of small-scale intermittency in 3-dimensional turbulence. *J. Fluid Mech.* **107**, 375–406 (1981).

24. She, Z. S., Jackson, E. & Orzag, S. Intermittent vortex structures in homogeneous isotropic turbulence. *Nature* **344**, 226–228 (1990).

25. Zaman, K. B. M. Q. & Hussain, A. K. M. F. Taylor hypothesis and large-scale coherent structures. *J. Fluid Mech.* **112**, 379–396 (1981).

26. Townsend, A. A. *The Structure of Turbulent Shear Flows* 2nd edn (Cambridge University Press, 1976).

27. Koeltzsch, K. On the relationship between Lagrangian and Eulerian time scale. *Atmos. Environ.* **33**, 117–128 (2005).

28. Burghelea, T., Segre, E. & Steinberg, V. Validity of the Taylor hypothesis in a random spatially smooth flow. *Phys. Fluids* **17**, 103101 (2005).

29. Del Alamo, J. C. & Jiménez, J. Estimation of turbulent convection velocities and corrections to Taylor's approximation. *J. Fluid Mech.* **640**, 5–26 (2009).

30. Lewis, G. S. & Swinney, H. L. Velocity structure functions, scaling, and transitions in high-Reynolds-number Couette-Taylor flow. *Phys. Rev. E* **59**, 5457–5467 (1999).

31. Uhlenbeck, G. E. & Ornstein, L. S. On the theory of Brownian motion. *Phys. Rev.* **36**, 823–841 (1930).

32. Dahm, W. J. A. & Southerland, K. B. Experimental assessment of Taylor's hypothesis and its applications to dissipation estimates in turbulent flows. *Phys. Fluids* **9**, 2101–2117 (1997).

33. Mesbah-Uddin, M., Perry, A. E. & Marusic, I. On the validity of Taylor's hypothesis in wall turbulence. *J. Mech. Eng. Res. Dev.* **19-20**, 57–66 (1997).

34. Tabeling, P., Zocchi, G., Belin, F., Maurer, J. & Willaime, H. Probability density functions, skewness, and flatness in large Reynold's number turbulence. *Phys. Rev. E* **53**, 1613–1621 (1996).

35. Ciliberto, S. *Turbulence* Vol. 341 (NATO ASI Series (Series B: Physics), 1995).

36. Cammusi, R., Barbagallo, D., Guj, R. & Stella, F. Transverse and longitudinal scaling laws in non-homogeneous low Re turbulence. *Phys. Fluids* **8**, 1181–1191 (1996).

37. A, N., G, W., Lempert, W., Miles, R. B. & Frisch, U. Transverse velocity measurements in turbulent flows using RELIEF technique. *Phys. Fluid Mech.* **339**, 287–307 (1997).

38. Cammusi, R. & Benzi, R. Hierarchy of transverse structure functions. *Phys. Fluids* **9**, 257–259 (1997).

39. Chen, S., Sreenivasan, K., Nelkin, M. & Cao, N. Z. Refined similarity hypothesis for transverse structure functions in fluid turbulence. *Phys. Rev. Lett.* **79**, 2253–2256 (1997).

40. Arneodo, A. et al. Structure functions in turbulence in various flow configurations at Reynolds numbers between 30 and 5000. *Europhys. Lett.* **34**, 411–416 (1996).

41. Saw, E.-W., Debue, P., Kuzzay, D., Daviaud, F. & Dubrulle, B. On the universality of anomalous scaling exponents of structure functions in turbulent flows. *J. Fluid Mech.* **837**, 657–669 (2018).

42. Arad, I., L'vov, V. S. & Procaccia, I. Anomalous scaling in anisotropic turbulence. *Physica A* **288**, 280–307 (2000).

43. Kurien, S., L'vov, V. S., Procaccia, I. & Sreenivasan, K. R. Scaling structure of the velocity statistics in atmospheric boundary layers. *Phys. Rev. E* **61**, 407–421 (2000).

44. Kurien, S. & Sreenivasan, K. R. Anisotropic scaling contributions to high-order structure functions in high-Reynolds-number turbulence. *Phys. Rev. E* **62**, 2206–2212 (2000).

45. Miller, J. D. et al. 100 kHz burst-mode particle image velocimetry: space-time correlations and considerations for spatial and temporal resolution. *Turbulence* 1–12 (2016).

46. Pope, S. B. *Turbulent Flows* (Cambridge University Press, 2000).

Author contributions

The authors contributed equally. S.R. and J.D.M. conducted the experiment and G.H.G. performed the data analysis. S.R. and G.H.G. wrote the paper.

Competing interests

The authors declare no competing interests.

Additional information

Supplementary information The online version contains supplementary material available at https://doi.org/10.1038/s42005-021-00528-0.

Correspondence and requests for materials should be addressed to S.R. or G.H.G.

Reprints and permission information is available at http://www.nature.com/reprints

Publisher's note Springer Nature remains neutral with regard to jurisdictional claims in published maps and institutional affiliations.

Terms and Conditions

Springer Nature journal content, brought to you courtesy of Springer Nature Customer Service Center GmbH ("Springer Nature").

Springer Nature supports a reasonable amount of sharing of research papers by authors, subscribers and authorised users ("Users"), for small-scale personal, non-commercial use provided that all copyright, trade and service marks and other proprietary notices are maintained. By accessing, sharing, receiving or otherwise using the Springer Nature journal content you agree to these terms of use ("Terms"). For these purposes, Springer Nature considers academic use (by researchers and students) to be non-commercial.

These Terms are supplementary and will apply in addition to any applicable website terms and conditions, a relevant site licence or a personal subscription. These Terms will prevail over any conflict or ambiguity with regards to the relevant terms, a site licence or a personal subscription (to the extent of the conflict or ambiguity only). For Creative Commons-licensed articles, the terms of the Creative Commons license used will apply.

We collect and use personal data to provide access to the Springer Nature journal content. We may also use these personal data internally within ResearchGate and Springer Nature and as agreed share it, in an anonymised way, for purposes of tracking, analysis and reporting. We will not otherwise disclose your personal data outside the ResearchGate or the Springer Nature group of companies unless we have your permission as detailed in the Privacy Policy.

While Users may use the Springer Nature journal content for small scale, personal non-commercial use, it is important to note that Users may not:

1. use such content for the purpose of providing other users with access on a regular or large scale basis or as a means to circumvent access control;

2. use such content where to do so would be considered a criminal or statutory offence in any jurisdiction, or gives rise to civil liability, or is otherwise unlawful;

3. falsely or misleadingly imply or suggest endorsement, approval , sponsorship, or association unless explicitly agreed to by Springer Nature in writing;

4. use bots or other automated methods to access the content or redirect messages

5. override any security feature or exclusionary protocol; or

6. share the content in order to create substitute for Springer Nature products or services or a systematic database of Springer Nature journal content.

In line with the restriction against commercial use, Springer Nature does not permit the creation of a product or service that creates revenue, royalties, rent or income from our content or its inclusion as part of a paid for service or for other commercial gain. Springer Nature journal content cannot be used for inter-library loans and librarians may not upload Springer Nature journal content on a large scale into their, or any other, institutional repository.

These terms of use are reviewed regularly and may be amended at any time. Springer Nature is not obligated to publish any information or content on this website and may remove it or features or functionality at our sole discretion, at any time with or without notice. Springer Nature may revoke this licence to you at any time and remove access to any copies of the Springer Nature journal content which have been saved.

To the fullest extent permitted by law, Springer Nature makes no warranties, representations or guarantees to Users, either express or implied with respect to the Springer nature journal content and all parties disclaim and waive any implied warranties or warranties imposed by law, including merchantability or fitness for any particular purpose.

Please note that these rights do not automatically extend to content, data or other material published by Springer Nature that may be licensed from third parties.

If you would like to use or distribute our Springer Nature journal content to a wider audience or on a regular basis or in any other manner not expressly permitted by these Terms, please contact Springer Nature at

onlineservice@springernature.com